

The role of dimers in complex forming reactions at low temperature: full dimension potential and dynamics of $(\text{H}_2\text{CO})_2 + \text{OH}$ reaction

Pablo del Mazo-Sevillano,^{*,[a]} Alfredo Aguado^{+, [a]} Alexandre Zanchet^{+, [b]} and Octavio Roncero^{*,[b]}

Dedicated to the 70th birthday of Prof. Pablo Villarreal

The $(\text{H}_2\text{CO})_2 + \text{OH}$ and $\text{H}_2\text{CO} \cdot \text{OH} + \text{H}_2\text{CO}$ reaction dynamics are studied theoretically for temperatures below 300 K. For this purpose, a full dimension potential energy surface is built, which reproduces well accurate ab initio calculations. The potential presents a submerged reaction barrier, as an example of the catalytic effect induced by the presence of the third molecule. However, quasi-classical and ring polymer molecular dynamics calculations show that the dominant channel is the dimer-exchange mechanism below 200 K, and that the reactive

rate constant tends to stabilize at low temperatures, because the effective dipole of either dimer is reduced with respect to that of formaldehyde alone. The reaction complex formed at low temperatures does not live long enough to produce complete energy relaxation, as assumed in statistical theories. These results show that the reactivity of the dimers cannot explain the large rate constants measured at temperatures below 100 K.

1. Introduction

The reaction of organic molecules with radicals, like OH, has been the subject of numerous experiments at low temperatures, using Laval expansions.^[1–7] The reaction rate constants thus measured show a V-shaped, non-Arrhenius behavior, with a minimum around 200 K, and a fast increase as temperature decreases –of one or even two orders of magnitude in some cases. This large rate constants at low temperatures have an enormous impact in the astrochemistry of cold molecular clouds, where organic molecules have been detected in UV-shielded cold cores at 10 K.^[8–11] The formation of organic molecules usually involves reactions with barriers, that cannot be overpassed in gas phase at low temperatures. For this reason, the usual assumption in astrochemical models, prior to these new observations, was that organic molecules are formed on ices, in cold molecular clouds at about 10 K,^[12,13] and then released to gas phase as they

evolve to hotter structures,^[14] such as hot cores and corinos, where they were observed.^[15–18]

These organic molecules have strong electric dipoles forming relatively strong bonds. Therefore, the chemical desorption at 10 K is not possible. Different alternatives have been proposed, such as chemidesorption,^[19,20] the incidence of cosmic rays^[21] and of secondary UV photons.^[22,23] The abundance of organic molecules in the interstellar medium (ISM) suggests a combined mechanism involving reactions on cosmic ices and gas phase re-processing. Understanding this mechanism is crucial for tracing the formation of prebiotic molecules during the star and planet formation cycle.^[24–27]

The high rate constant of organic molecules reacting with radicals at low temperature can facilitate gas phase routes for the formation of new molecules. These reactions involve the formation of long-lived complexes between the reactants, followed by the tunneling process that leads to the formation of products.^[5,6]

Several statistical theories, including transition state theory (TST) and RRKM methods, have been unable to quantitatively reproduce the observed reaction rate of the prototypical $\text{CH}_3\text{OH} + \text{OH}$ reaction at low temperatures in the gas phase. However, the inclusion of pressure effects in these theories can lead to results that are consistent with experimental measurements.^[7,28,29] Also Siebrand *et al.*^[30] proposed the possibility of the formation of $(\text{CH}_3\text{OH})_2$ dimers which react with OH as a possible explanation for the rise of the rate constant as temperature decreases below 100 K. Here we assume, that the formation of dimers is a microscopic analogue of the pressure effect, in which a dimer is first formed, followed by a collision with OH radical. At this point, it is important to notice that recent simulations using ring

[a] Dr. P. del Mazo-Sevillano, Dr. A. Aguado^{*}
Unidad Asociada UAM-IFF-CSIC, Departamento de Química Física Aplicada,
Facultad de Ciencias M-14, Universidad Autónoma de Madrid, 28049,
Madrid, Spain
E-mail: pablo.delmazo@uam.es
[b] Dr. A. Zanchet,⁺ Dr. O. Roncero
Instituto de Física Fundamental (CSIC), c/ Serrano 123, 28006 Madrid
(Spain)
E-mail: octavio.roncero@csic.es

[*] These authors contributed equally to this work.

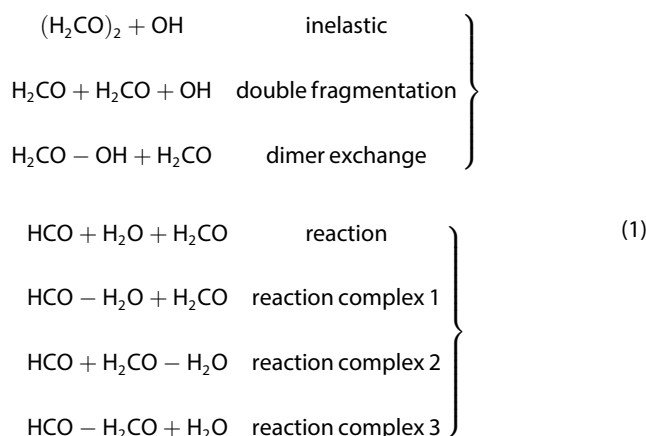
© 2023 The Authors. ChemPhysChem published by Wiley-VCH GmbH.
This is an open access article under the terms of the Creative Commons
Attribution Non-Commercial NoDerivs License, which permits use and
distribution in any medium, provided the original work is properly cited,
the use is non-commercial and no modifications or adaptations are
made.

polymer molecular dynamics (RPMD) method, combined with TST at low temperatures, were able to reproduce the experimental rate constants for the $\text{CH}_3\text{OH} + \text{OH}$ reaction in the 10–300 K temperature interval^[31,32] in gas phase, without having to consider high pressure effects. However, very long lived complexes were formed, which could justify the existence of secondary collisions, or in other words, pressure effects.

The ISM is a very diluted environment, with very low density, so pressure effects are expected to be absent there. Consequently, it is of paramount importance to determine the zero-pressure reaction rate constants. This underscores the importance of investigating the role of pressure effects in Laval experiments. In these types of experiments, expansion complexes can form, which may undergo secondary collisions, mimicking the effects of pressure at a microscopic level. In such expansions, the buffer gas, such as He, is typically the most abundant species, while the second most abundant are organic molecules (OMs), such as methanol or formaldehyde. The radical species, which is formed by photolysis, is typically the least abundant species in these experiments. Its abundance is monitored by Laser-Induced Fluorescence (LIF) to determine the reaction rate constant. Hence, the most abundant complexes formed in these experiments are expected to be those of OMs with He. Recent studies on formaldehyde (H_2CO)-He complexes have shown that they are stable at temperatures below 50 K.^[32] The reactivity of these complexes was investigated using quasi-classical trajectories (QCT), but it was found that the low interaction between He and formaldehyde did not strongly modify their reactivity.^[32]

In this study, we aim to build upon the previous work on the reactivity of dimers in the interstellar medium by focusing on the $(\text{H}_2\text{CO})_2$ dimer. To achieve this, we have developed a full dimensional potential energy surface (PES) and conducted a comprehensive study of the reaction dynamics. The idea of dimers as intermediates in reactions involving organic molecules and OH radicals was initially proposed by Siebrand and co-workers.^[30] Their study employed a statistical approach, which involved the separate evaluation of different steps such as complex formation, redissociation, and reaction pathways to determine individual rate constants. The total reaction rate constant was obtained by solving the master equations.

In this work, our objective is to investigate the full dynamics of the $(\text{H}_2\text{CO})_2 + \text{OH}$ reaction and compare its reaction rate with that of the monomer. Our aim is to develop a microscopic model for pressure effects and clarify their impact in the CRESU expansions at temperatures below 100 K, which are relevant to the ISM. The reaction of the $(\text{H}_2\text{CO})_2$ dimer with OH can lead to various possible products



which are grouped in two sets, depending on whether there is or not reaction between any formaldehyde and OH. The formation of the formic acid presents a higher reaction barrier, and this channel remains closed at the low temperature considered in this work.

In the entrance channel, with no reaction forming HCO or H_2O products, there are also different exit channels, the dimer exchange forming $\text{H}_2\text{CO}-\text{OH}$ and the double fragmentation, which results in the separation of all three molecules. The second objective of this work is to address the cluster formation in Laval expansions when binary gas mixtures are considered. In this situation recent experiments have determined that the presence of secondary species act as a catalyst for the dimers or larger complexes of primary species.^[33–35] To this aim, here we shall also focus on the dimer exchange rate constant, and its dependence with temperature, to provide valuable data to model the complexation kinetics.

In pursuit of these goals, in this work we develop a full-dimensional potential model, described in Section 2. In Section 2.1 we focus on the accuracy of our H_2CO dimers description and highlight the key characteristics of the PES that are significant for reaction dynamics. Finally, in Section 3 we provide a quasi-classical trajectory (QCT) and ring polymer molecular dynamics (RPMD) study of the reaction, discussing some of their limitations in this kind of systems.

2. The Global Potential Energy Surface

In building the global potential energy surface we assume that the extra H_2CO can be treated as a perturbation of the $\text{H}_2\text{CO} + \text{OH}$ (monomer) PES, hence only the interaction between the former and the latter molecules has to be included. Thus, a good approach is to describe the reactions in Eq. 1 as

$$\begin{aligned}
 V((\text{H}_2\text{CO})_2 + \text{OH}) &= E_0((\text{H}_2\text{CO})_2 + \text{OH}) \\
 &+ V^{6C}([\text{H}_2\text{CO}]_A + \text{OH}) \\
 &+ V^{6C}([\text{H}_2\text{CO}]_B + \text{OH})
 \end{aligned} \quad (2)$$

where V^{6C} ($X=A$ or B) is a 6-body neural-network (NN) term which was previously developed to describe the corresponding reaction of the monomer.^[36] In Eq. 2, E_0 represents the lowest eigenvalue of the 9×9 reactive force-field like potential matrix, whose diagonal elements correspond to the rearrangement channels considered in the reaction. These diagonal terms provide the zero-order description of the inter and intramolecular potential interactions among all the fragments of each rearrangement channel:

$$H_0(i, i) = \begin{pmatrix} [\text{H}_2\text{CO}]_A + [\text{H}_2\text{CO}]_B + \text{OH} \\ [\text{H}^1\text{CO}]_A + \text{H}_2\text{O} + [\text{H}_2\text{CO}]_B \\ [\text{H}^2\text{CO}]_A + \text{H}_2\text{O} + [\text{H}_2\text{CO}]_B \\ [\text{H}_2\text{CO}]_A + \text{H}_2\text{O} + [\text{H}^1\text{CO}]_B \\ [\text{H}_2\text{CO}]_A + \text{H}_2\text{O} + [\text{H}^2\text{CO}]_B \\ [\text{H}^1\text{COOH}]_A + \text{H} + [\text{H}_2\text{CO}]_B \\ [\text{H}^2\text{COOH}]_A + \text{H} + [\text{H}_2\text{CO}]_B \\ [\text{H}_2\text{CO}]_A + \text{H} + [\text{H}^1\text{COOH}]_B \\ [\text{H}_2\text{CO}]_A + \text{H} + [\text{H}^2\text{COOH}]_B \end{pmatrix} \quad (3)$$

The off-diagonal elements of the force-field potential matrix, which are effective couplings among the rearrangement channels producing a smooth transition between them, are identical to those from the $\text{H}_2\text{CO} + \text{OH}$ PES.^[36] These couplings are Gaussian functions depending on the energy difference between the diagonal energies of the two channels, multiplied by switching functions, which are optimized to match the height and the shape of the saddle points.^[37]

The diagonal elements in Eq. 3 describe the potential energy of each of the three independent monomers considered (denoted by $V_A + V_B + V_C$, where $A, B, C = \text{H}_2\text{CO}, \text{OH}, \text{HCO}, \text{H}_2\text{O}$ and HCOOH) together with the interactions among them ($W_{AB} + W_{BC} + W_{AC}$), which include the long-range interactions of the reactants.^[36,37] Each monomer PES is represented with a NN potential as described in Ref. [36], together with the interaction terms $W_{\text{H}_2\text{CO}-\text{OH}}$, $W_{\text{HCO}-\text{H}_2\text{O}}$ and $W_{\text{HCOOH}-\text{H}}$. In this work we have included the new interaction potentials describing the remaining dimers. Specifically, we have performed an analytical fit for the formaldehyde dimers ($W_{\text{H}_2\text{CO}-\text{H}_2\text{CO}}$), $W_{\text{H}_2\text{CO}-\text{HCO}}$, and $W_{\text{H}_2\text{CO}-\text{H}_2\text{O}}$. However, we have chosen to describe the potentials associated with the formic acid products in a separate report for clarity, as these products are not formed under the current simulation conditions. In all cases, the dimer PESs developed are based on new RCCSD(T)-F12a calculations, with the MOLPRO package^[38] and using the cc-pVDZ-F12 basis set,^[39] i.e. keeping the same level of theory employed before^[36,37].

2.1. Dimers and trimers

The analytical interaction potential $W_{\text{H}_2\text{CO}-\text{H}_2\text{CO}}$ is obtained by summing up the pair potentials between the atoms from each monomer. In order to capture the anisotropy of the potential, additional interaction centers are also considered at fictive points located at the midpoint between the O–H and H–H atoms of each formaldehyde unit. Different functions are employed for each pair interaction. Attractive Morse potentials are utilized to describe the interaction between oxygen with carbon and hydrogen. Repulsive exponential or polynomial functions are used to describe the interactions between carbon with hydrogen, carbon-carbon, oxygen-oxygen, and hydrogen-hydrogen. The interactions between the atoms and the fictive points are modeled by combining Morse functions and Gaussian functions, while simple Gaussian functions are used to describe all pair interactions involving the fictive points. In the case of the interaction between the fictive points associated to the OH mid distance, a damping function is employed to modulate the shape of the Gaussian along the interaction distance. These functions are well behaved and were elected to avoid any artifacts in the interaction potential. To complete the sum of pair potentials, fictive charges are allocated to each atom to obtain a good long range interaction and in particular, a good description of the dipole-dipole interaction. In order to avoid numerical problems, no charges are assigned to the fictive interaction points and a switching function is employed to smoothly damp the electrostatic term when the two monomers get too close. Otherwise, Coulomb interaction may artificially diverge for short distances.

By construction, $W_{\text{H}_2\text{CO}-\text{H}_2\text{CO}}$ intermolecular force field potential is defined by 59 parameters. These parameters are optimized by minimizing the difference with *ab initio* interaction potential, subtracting the energy of each monomer.^[36] Around 6000 geometries were randomly generated keeping both monomers in their equilibrium geometries and then used for a first optimization of the parameters. After that, 4000 additional points were generated running classical trajectories to account for the vibrational motion of both formaldehydes. To increase the accuracy in the attractive regions, different weights have been considered in the optimization procedure. The geometries whose *ab initio* interaction potential is lower than -0.04 eV are weighted by a factor of 50, and those with energies lower than $+0.15$ eV with a factor of 5. In contrast, when the *ab initio* interaction potential is higher than $+2.5$ eV, the corresponding geometries are weighted by a factor of 10^{-2} and when it is higher than $+5$ eV, the weights are further diminished to 10^{-5} . Points with interaction energies higher than $+8$ eV were excluded. The weighted RMS error obtained applying this procedure is 20 meV.

Table 1 presents a comparison between our potential energy surface and previous *ab initio*^[40,41] and experimental results^[42,43] regarding the stationary points of the H_2CO dimer (whose geometries are shown in Figure 1). Our potential energy surface shows an excellent agreement with previous results, both in terms of energy and structure – only the C_{2h} (stack) structure presents a larger disagreement. Upon performing a

Table 1. Principal characteristics of the five stationary points of the dimer analytical PES and comparison with optimized *ab initio* values and available experimental data. *Ab initio* values of this work at CCSD(T)-F12/VDZ-F12 level are shown as well as the results at CCSD(T)/CBS level from Dolgonos^[40] (referred as a) and at CCSD(T)-F12/haTZ level from Van Dornshuld et al.^[41] (referred as b). Experimentally derived data are taken from the works of Lovas et al.^[42] (referred as c) and Barry et al.^[43] (referred as d). *Ab initio* results for the ZPE are calculated within the harmonic approximation. The theoretical harmonic D_0 are obtained by the difference of D_e and the harmonic ZPE. A D_0 value of our analytical fit estimated with Path Integral method is also shown and is marked with *. The nature of the stationary point is indicated by the number of imaginary frequencies ν_i .

Dimer	Parameter	Analytical PES (This work)	<i>ab initio</i> (This work)	<i>ab initio</i> (Other works)	Exp.
C_s	D_e (meV)	195	190	194 ^a , 199 ^b	
	ZPE (meV)	80	59	66 ^a , 71 ^b	
	D_0 (meV)	129*	–	128 ^a , 128 ^b	97 ^d
	R_{CM} (Å)	2.95		2.89 ^b	3.046 ^c
	$R_{C_1O_2}$ (Å)	2.74	–		2.98/2.82 ^c
	$R_{O_1H_2}$ (Å)	2.46	–		2.18/2.46 ^c
	ν_i	0		0	–
C_{2h} (planar)	D_e (meV)	162	158	160 ^a , 163 ^b	–
	R_{CM} (Å)	3.27		3.30 ^b	–
	ν_i	0	–	0	–
C_{2h} (stack)	D_e (meV)	96		114 ^b	–
	R_{CM} (Å)	3.42		3.14 ^b	–
	ν_i	3	–	3	–
C_{2v} (trans)	D_e (meV)	102	106	110 ^b	–
	R_{CM} (Å)	4.35		4.29 ^b	–
	ν_i	1	–	1	–
C_{2v} (cis)	D_e (meV)	102	102	106 ^b	–
	R_{CM} (Å)	4.35		4.35 ^b	–
	ν_i	2	–	2	–

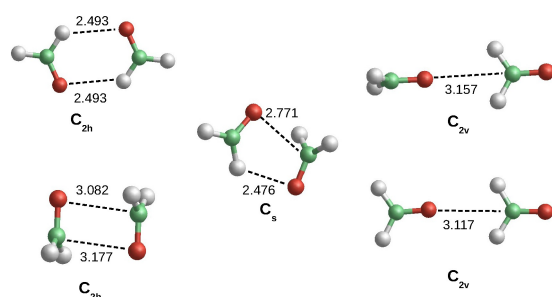


Figure 1. Structures and symmetry group of the formaldehyde dimer stationary points.

normal mode analysis of the stationary points, we confirm that only the C_s and C_{2h} (planar) stationary points are minima, with all their normal mode frequencies being real. Conversely, all other stationary points correspond to first or higher order transition states. The number of imaginary frequencies found with our potential energy surface matches the results reported by Van Dornshuld *et al.*,^[41] where C_{2h} (stack), C_{2v} (trans) and C_{2v} (cis) correspond to third, first, and second order transition states, respectively.

Due to the large anharmonic nature of the dimer intermolecular interactions, harmonic zero-point energies (ZPE) cannot be employed to compare with experimental results, even with the best *ab initio* calculation. Instead, in this work we use Path Integral Molecular Dynamics (PIMD) method to calculate the exact ZPE and the dissociation energy of the dimers. For that, the average energy of the dimer is calculated at different temperatures, as shown in Figure 2. The virial energy estimator^[44] is used with an MPI parallelized in-house code,^[45] ZPIMD, based on RPMDrate.^[46] To extract the intermolecular

dissociation energy, D_0 , we performed two sort of calculations, one with two formaldehydes constrained to be separated by 50 Å, and the second with no restrictions, giving rise to the dimer. At 1 K, the value of D_0 of the complex estimated as the difference in the average energies is $D_0(T = 1 \text{ K}) = 0.129 \text{ eV}$, as compared to 0.101 eV obtained in the harmonic approximation. D_0 decreases with temperature for $T > 200 \text{ K}$, and reduces to $D_0(T = 200 \text{ K}) = 0.120 \text{ eV}$ and $D_0(T = 300 \text{ K}) = 0.070 \text{ eV}$. According to Barry *et al.*,^[43] the intermolecular dissociation energy D_0 was found to be $0.097 \pm 0.015 \text{ eV}$ at 300 K, using pressure broadening cross sections determined from cavity enhanced absorption spectroscopy experiments. Our calculations show that the D_0 values obtained for 200 K and 300 K are in between the experimental value. However, it is important to note that even slight temperature variations within this range can lead to significant changes in the determination of D_0 .

In Figure 2, the origin of energy is set at the equilibrium geometry of the H_2CO and OH, with the two or three fragments at long distances, $\approx 50 \text{ Å}$. The average energy for each case is then approximately the ZPE at 1 K. For $(H_2CO)_2$ dimer, we obtain a ZPE of 1.293 eV, which is twice the ZPE of H_2CO minus the dissociation energy of the dimer, $D_0(T)$. From the dissociation energy, $D_0(T = 0 \text{ K}) = 0.129 \text{ eV}$, and $D_e(C_s) = 0.192 \text{ eV}$, we obtain a ZPE of 63 meV for the intermolecular interaction of the dimer. Since $D_0 \approx 0.129 \text{ eV}$ at $T < 200 \text{ K}$, in this temperature interval the two minima, C_s and C_{2h} (planar), are sampled.

Experimentally, the rotational^[42] and vibrational^[47] spectra indicate that the structure corresponds to the C_s conformation of the dimer, which is also the most stable conformation. In their work, Lovas *et al.*^[42] proposed two possible solutions matching the inferred momenta of inertia, $R_{C_1O_2} = 2.98 \text{ Å}$ and $R_{O_1H_2} = 2.18 \text{ Å}$, or $R_{C_1O_2} = 2.82 \text{ Å}$ and $R_{O_1H_2} = 2.46 \text{ Å}$. The minimum

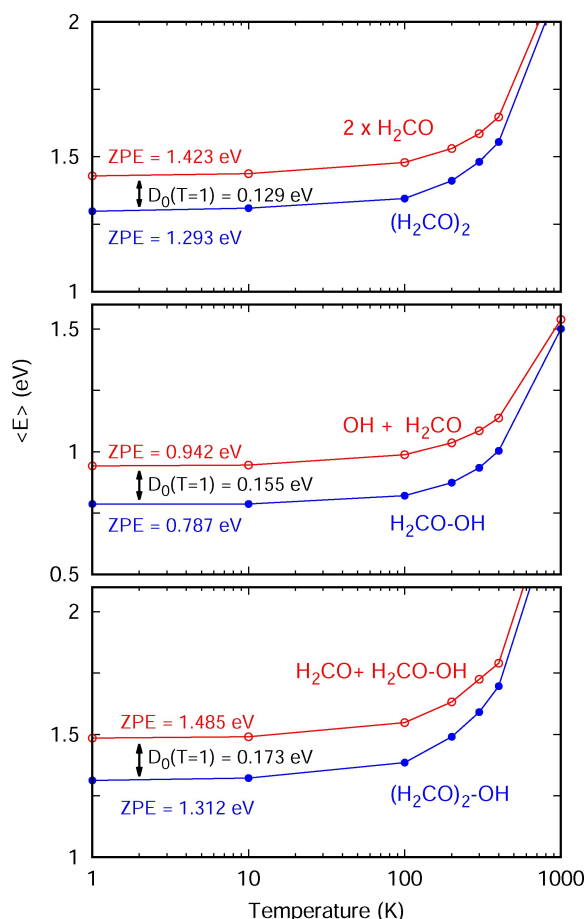


Figure 2. Average energy obtained with the PIMD method as a function of temperature for (H₂CO)₂ dimer (top panel), H₂CO–OH dimer (middle panel) and OH–(H₂CO)₂ trimer (bottom panel). The number of beads used in the calculations are 30720, 15360, 1536 and 768 for 1, 10, 100 and 200 K. For T ≥ 300 K, $n_{\text{beads}} = 480$. The ZPE of H₂CO is 0.712 eV and that of OH is 0.230 eV

of the PES calculated in this work is close to the second pair of distances estimated experimentally suggesting that this conformation is effectively the most stable, and that the description of the analytic PES is rather accurate.

The anharmonic ZPE and D₀ for the H₂CO–OH dimer and (H₂CO)₂–OH trimer is also plot in Figure 2. The H₂CO–OH dimer has a lower energy than (H₂CO)₂ dimer, by approximately 0.050 eV, being the reactant with the lowest energy in the system. The (H₂CO)₂–OH trimer is bound by approximately 0.165 eV. All these features are described below.

2.2. Features of the global PES

The global potential energy surface for the H₂CO dimer reaction is constructed as a combination of our previous fit for the monomer reaction (H₂CO + OH^[36]) and the above described interaction terms between the different fragments. In this case we find a much more complex structure with many local minima and transition states along reaction paths.

On the reactants side, we have characterized three trimer minima ((H₂CO)₂–OH), the lowest with an energy of –0.486 eV (1.320 eV including the anharmonic ZPE) with respect to the total dissociation (zero of potential energy and 1.653 eV including the anharmonic ZPE). All of the three minima present a geometry closely related to the reactant's minima for the monomer reaction, and only the relative position of the second H₂CO changes, in all cases close to the C_s dimer minima with slight angular variations due to the OH symmetry breaking.

The global minimum on the reactants side is connected to a transitions state lying at an energy of –0.319 eV. This is a significant result as the transition state is found to be below the energy of the dimer + OH, contrary to the monomer case where the TS is slightly above the asymptote (see Figure 3). That means that the presence of the H₂CO dimer is acting as a catalyst to the reaction, as the non-reactive H₂CO stabilizes the TS via H-bond between its oxygen and the OH hydrogen.

The minimum energy path for the dimer reaction to the formation of HCO + H₂O is presented in the inset of Figure 3 along with the energies computed at RCCSD(T)-F12a/cc-pVDZ–F12 level of theory. In general, we find a good agreement, given the large dimensionality of the system, with an energy difference in the transition state region of about 60 meV. This difference is not expected to play a significant role since the barrier is already submerged with respect to the asymptote and the H₂CO dimer + OH energy.

The second path investigated in this study involves the reaction between the H₂CO–OH complex and a second H₂CO molecule, which shares some similarities with the first reaction pathway. The H₂CO–OH complex is slightly lower in energy than the H₂CO dimer at –0.195 eV. Following this point, both reaction pathways converge at the same trimer minimum energy level of –0.486 eV and proceed towards the same transition state.

To summarize, the new PES constructed for studying the reaction of (H₂CO)₂ dimer with OH and H₂CO–OH + H₂CO reveals

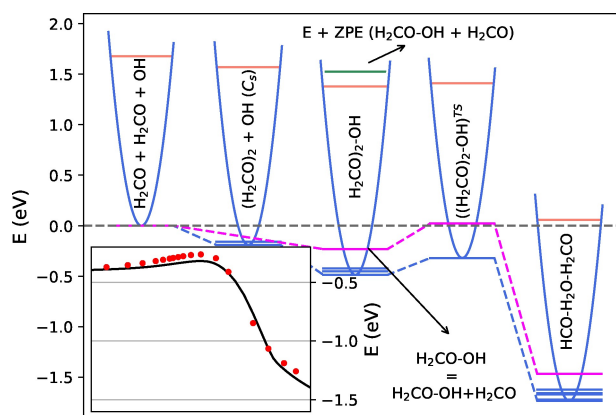


Figure 3. Minimum energy path for the dimer (blue) and monomer (magenta) H₂CO reaction with OH. The harmonic ZPEs of the dimer species are indicated with red lines for the most stable species along the reaction. The inset represents a comparison between the PES (black solid line) and RCCSD(T)-F12a/cc-pVDZ–F12 calculations along the reaction coordinate in the TS region.

that the reaction has a saddle point at -0.319 eV relative to the $\text{H}_2\text{CO} + \text{H}_2\text{CO} + \text{OH}$ asymptote, which is considered as the zero of energy. This saddle point is lower than that of the monomer, indicating that the environment (represented here by the second H_2CO molecule) has a catalytic effect. The saddle point for the dimer reaction is located below the energy of the $(\text{H}_2\text{CO})_2 + \text{OH}$ reactants (with and without zero-point energy), making it a submerged barrier.

We should remark here, that the RCCSD(T)-F12a calculations performed over the reaction path extracted from our analytical potential confirm the catalytic effect associated to the polarisation induced by the second formaldehyde. This validates that our initial assumption of incorporating its effect in the zero-order force-field matrix is a reasonable approximation.

3. QCT calculations

The $(\text{H}_2\text{CO})_2 + \text{OH}$ temperature dependent reaction rate constant has been computed as:

$$k(T) = q_e(T) \sqrt{\frac{8k_B T}{\pi \mu}} \pi b_{\max}^2(T) P_r(T), \quad (4)$$

where $\mu = m_{\text{OH}} m_{(\text{H}_2\text{CO})_2} / (m_{\text{OH}} + m_{(\text{H}_2\text{CO})_2})$, $b_{\max}(T)$ is the maximum impact parameter and the reaction probabilities for each product channel $P_r(T)$ have been calculated with quasiclassical trajectories (QCT) method. In Eq. 4 the electronic partition function is defined as

$$q_e(T) = [1 + \exp(-200.3/T)]^{-1}, \quad (5)$$

in which it is assumed that only the two lower spin-orbit states react – those that correlate with the ground state of $\text{OH}(^2\Pi_{3/2})$.

The calculations are performed with the MDwQT code.^[5,48,49] The Hamilton equations are integrated in time in Cartesian coordinates with the step adaptive Adams-Bashforth-Moulton predictor corrector method.^[50] Initial conditions are sampled with the usual Monte Carlo method,^[51] according to the following prescription. An adiabatic switching method^[52–54] is used to determine the initial intramolecular positions and velocities of OH and $(\text{H}_2\text{CO})_2$ dimer (and H_2CO and $\text{H}_2\text{CO}-\text{OH}$), independently for the ground vibrational and rotational state. This step is critical to describe the dimers, where the harmonic frequencies would add a huge energy excess to the weakly bound system. Thus, the initial conditions of the formaldehyde dimer are taken from a single trajectory with a final energy of 1.287 eV (the average dimer energy at 1 K computed with PIMD). For the OH, the initial conditions are taken from a trajectory with a final energy of 0.230 eV – its ground rovibrational eigenvalue.

At this geometry, a rotational quantum number is chosen randomly according to a Boltzmann distribution for the given temperature, and the principal axis of each reactant are rotated by three random Euler angles. The initial distance between the center-of-mass of the reactants – H_2CO dimer and OH – is set to $80 a_0$ and the trajectories are stopped if any interatomic

distances is larger than $90 a_0$. The initial impact parameter is sampled between 0 and $60 a_0$, according to a quadratic distribution. For each translational/rotational temperature, about 10^6 trajectories are run, with a time step of 1 fs, to obtain the individual rates.

For the final analysis, the internal rovibrational energies of all fragments are calculated, with their translational energy subtracted. Only trajectories with a total internal energy higher than the corresponding ZPE are included in the count.^[55] The ZPE correction is not applied to the inelastic channel (back to $(\text{H}_2\text{CO})_2 + \text{OH}$) nor to the products ($\text{HCO} + \text{H}_2\text{O} + \text{H}_2\text{CO}$), and is only applied to the total fragmentation ($\text{H}_2\text{CO} + \text{H}_2\text{CO} + \text{OH}$) and the exchange dimer mechanism ($\text{H}_2\text{CO}-\text{OH} + \text{H}_2\text{CO}$). Thus, after the ZPE correction, the total fragmentation channel is nearly suppressed at low temperature (as it should below 100 K), while for the exchange dimer mechanism the number of final trajectories is reduced to approximately a half. In addition, the minimum distance among the reactants, R_{\min} , is evaluated along the reaction. If there is any rearrangement of the reactants with $R_{\min} > 15 \text{ \AA}$ the trajectory is discarded. These two final conditions are aimed to minimize the nonphysical breaking of dimers when the energy flows from the high frequency modes to the low frequency intermolecular modes of the dimer, i.e. the dimers stability in QCT calculations described in more detail below.

3.1. Classical stability of dimers

The initial conditions of the H_2CO dimer and $\text{H}_2\text{CO}-\text{OH}$ are prepared using the adiabatic switching method, targeting an internal energy equal to the anharmonic ZPE calculated with the PIMD method, i.e. an energy of 1.293 eV for the former. With it, we intend to obtain initial conditions with a classical energy comparable to the energy of the desired quantum state. However, given the classical propagation of the trajectory and that the dissociation energy of the complexes is significantly lower than their internal energy, there is no guarantee that there will not be an unrealistic energy transfer (compared to the quantum case) that will dissociate the fragments, leaving them with an internal energy below its ZPE.

In particular, using several initial conditions for the complexes, obtained with the adiabatic switching method, we check that in most cases the dimer breaks, for sufficiently long integration time, and systematically with at least one of the subunits with an energy below the ZPE requirements.

In Figure 4 the main results of this stability analysis are presented. Figure 4 a) presents the percentage of broken complex with time. A complex is considered to be broken whenever the distance between the centers of mass of both monomers is larger than 35 \AA , given some roaming behavior where the subunits fly apart and come back together due to the long range, dipole-dipole interactions among them. The $\text{H}_2\text{CO}-\text{H}_2\text{CO}$ appears to be much more stable, in this classical propagation, than the $\text{H}_2\text{CO}-\text{OH}$. While a large fraction of the former remains bounded until at least 20 ps, the latter usually breaks in the first few ps of the propagation. In the case of the

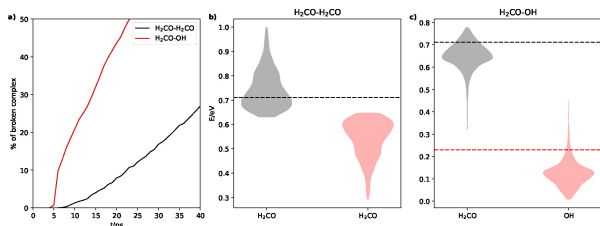


Figure 4. Stability analysis of $\text{H}_2\text{CO}-\text{H}_2\text{CO}$ and $\text{H}_2\text{CO}-\text{OH}$ complexes. In panel a) the percentage of trajectories started from either of the complexes that break within a propagation time is presented. Panels b) and c) represent the rovibrational energy distributions of the broken subunits for the H_2CO dimer and $\text{H}_2\text{CO}-\text{OH}$ complex, respectively. Panel b) shows the H_2CO subunits being divided into those with the highest (black) and lowest (red) energy. Horizontal lines indicate the ZPE of the H_2CO and OH.

$(\text{H}_2\text{CO})_2$, the stability time of around 20 ps is sufficiently long to allow the OH to reach the dimer and collide with it. In contrast, the stability time of $\text{H}_2\text{CO}-\text{OH}$ is too short and does not allow to classically simulate its collision with a formaldehyde. Figures 4 b) and c) analyze the rovibrational energy distributions for the broken subunits in the H_2CO dimer and $\text{H}_2\text{CO}-\text{OH}$ complexes. In Figure 4 b), the black and red violins represent the H_2CO molecule with the highest and lowest internal energy, respectively. In all the cases, one of the H_2CO subunits leaves with an energy below the ZPE, due to unrealistic energy transfer from rovibrational modes to translation. The energy asymmetry is more noticeable in the $\text{H}_2\text{CO}-\text{OH}$ complex (Figure 4 c)), with the H_2CO subunit exhibiting a preference for larger rovibrational energies, while the OH subunit tends to have lower energies. The different behavior in both distributions can be explained by a more efficient energy transfer between equivalent H_2CO subunits in the H_2CO dimer, producing a much more symmetric energy distribution, while the $\text{H}_2\text{CO}-\text{OH}$ complex allows a more efficient energy transfer to dissociation modes (translation).

For this reason, only the reaction between the H_2CO dimer and OH will be studied at a QCT level, as unreliable results would be obtained for the latter reaction.

To minimize the dimer stability problem, in the adiabatic switching method the initial vibrational conditions are chosen to minimize the energy difference with the quantum PIMD ZPE and maximize the lifetime of the trajectory.

3.2. $(\text{H}_2\text{CO})_2 + \text{OH}$ QCT reaction rates

The ZPE-corrected total reaction rate constant, corresponding to the sum over the four reactive channels in Eq. 1, are shown in the bottom panel of Figure 5, and compared with those obtained previously for the monomer.^[36] In the two cases, the rate constant increases with decreasing temperature, a typical behavior of strong long range dipole-dipole interaction. This is explained by the attraction exerted by long range interactions, which are able to deviate trajectories with very large impact parameter, as reported previously.^[37] Since this effect increases with decreasing energy or temperature, so does the QCT energy rate.

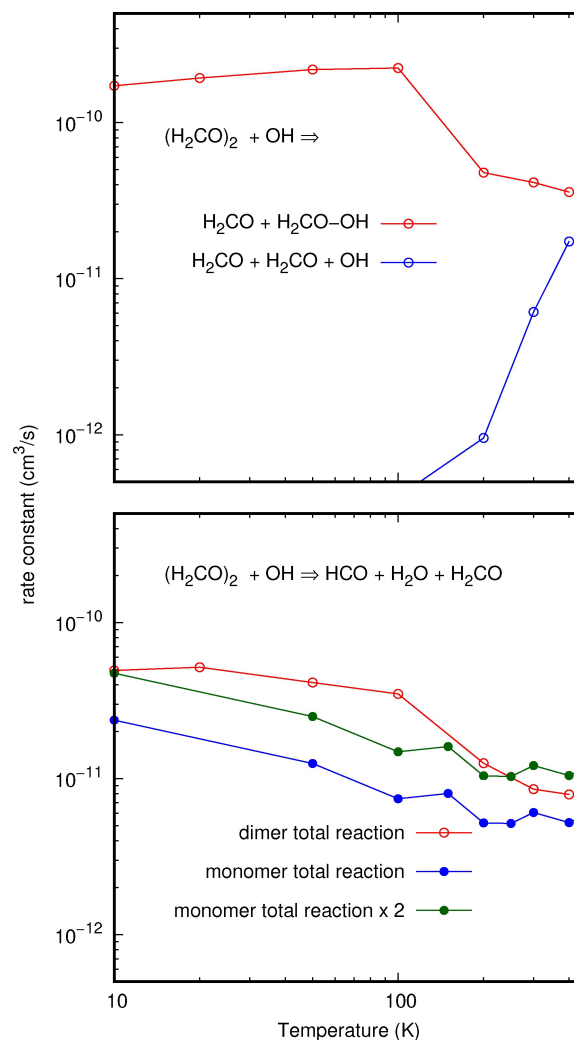


Figure 5. Bottom panel: Total reaction rate constants obtained for the $(\text{H}_2\text{CO})_2 + \text{OH}$ collisions as a function of temperature obtained with the QCT method. QCT results obtained for the monomer in $\text{H}_2\text{CO} + \text{OH}$ collisions are also shown for comparison.^[36] Top panel: rate constant for the formation of $\text{H}_2\text{CO}-\text{OH} + \text{H}_2\text{CO}$, dimer exchange, and total fragmentation in $\text{H}_2\text{CO} + \text{H}_2\text{CO} + \text{OH}$.

The rise of the rate constant with decreasing temperature, however, stops for the dimer at 50–100 K, what is surprising since the reaction barrier for the dimer is submerged, while for the monomer is not. Since the rise is due to the long range interaction, this effect is mostly attributed to the reduction of the effective dipole moment of the dimer. The H_2CO dipole moment is mainly oriented along the CO bond. The minimum energy structure of $(\text{H}_2\text{CO})_2$ dimer is the C_s conformation where the two CO bonds are parallel but oriented in opposite directions, thus reducing the effective dipole moment.

The reactivity of the dimer is larger than that of the monomer in the whole temperature range studied. This is attributed to the lowering of the saddle points for the reaction, which are stabilized with respect to those of the monomer by forming complexes. This effect can be viewed as a catalytic effect, given that the second formaldehyde does not react.

The dimer/monomer ratio of the rate constants, $R_{D/M}$, depends on temperature. The formation of a dimer reduces the concentration of formaldehyde by a factor of 2. Therefore, $R_{D/M} > 2$ could explain the fast increase of the reactive rate constant for low temperatures. However, $R_{D/M} < 2$ would produce a reduction of the effective rate constant measured. At 100 K, $R_{D/M}$ is about a factor of 5, but at $T = 10$ K, $R_{D/M} \approx 2$ and therefore cannot be the responsible for the significant increase observed at such low temperatures.

On the top panel of Figure 5 the rate for the exchange mechanism, producing $\text{H}_2\text{CO}-\text{OH}$ dimer, is shown. This rate increases from 400 K to 100 K, while below 100 K it slightly decreases with temperature. The behavior below 100 K is also attributed to the lower effective dipole moment of the formaldehyde dimer as temperature decreases. On the contrary, the rate constant for the fragmentation in three fragments $\text{H}_2\text{CO} + \text{H}_2\text{CO} + \text{OH}$ decreases with decreasing energy. This is explained by the reduction of the available energy needed to produce the double fragmentation in three fragments. It should be noted that when not correcting the ZPE of products, the three fragments channel becomes dominant, demonstrating the nonphysical energy flow from the intramolecular monomer's energy to the intermolecular degrees of freedom of the dimer. On the contrary, the other channels shown in Figure 5 are only slightly affected by the ZPE correction.

It is important to note that the rate constant for the dimer exchange, forming $\text{H}_2\text{CO}-\text{OH}$ complex, is about 4 times larger than the reactive one, forming $\text{HCO} + \text{H}_2\text{O} + \text{H}_2\text{CO}$, in all the temperature interval studied. Under complete randomization conditions assumed in RRKM theory, when forming the $(\text{H}_2\text{CO})_2-\text{OH}$ complex, the main dissociation channel would be the $\text{HCO} + \text{H}_2\text{O} + \text{H}_2\text{CO}$ products, since the reaction barrier (at -0.150 eV with respect to $(\text{H}_2\text{CO})_2 + \text{OH}$ reactants, considering PIMD ZPE) is lower than the $\text{H}_2\text{CO}-\text{OH} + \text{H}_2\text{CO}$ asymptotic energy (of -0.020 eV considering PIMD ZPE). This result is taken as an indication that the randomization is not complete, and that the dynamics favor the dimer exchange to form H_2CO complexes.

This study of the reaction dynamics of $(\text{H}_2\text{CO})_2$ with OH, seems to indicate that it does not explain by itself the increase of the reaction rate constant (forming $\text{HCO} + \text{H}_2\text{O}$ products) but, instead it mainly forms the $\text{H}_2\text{CO}-\text{OH}$ complex. Now the question is whether there is a possibility for the $\text{H}_2\text{CO}-\text{OH}$ complex to undergo a second collision with another H_2CO molecule and if this could explain the surge in reactivity.

This study with QCT method is not afforded here, because of the lack of stability of the $\text{H}_2\text{CO}-\text{OH}$ complex discussed above. Moreover, when studying $\text{H}_2\text{CO}-\text{OH} + \text{H}_2\text{CO}$ collision, the initial dimer not only breaks but also reacts at very long distances from the second formaldehyde. The presence of the second formaldehyde, even at very long distances (longer than 30 Å) induces the reaction, what is taken as an artifact. This artifact can be discarded by removing those trajectories that react at very long distances. At low temperatures, the combination of the ZPE correction and the aforementioned restriction severely reduces the statistics, which makes it challenging to obtain meaningful results. The root of this issue

is traced back to the QCT method's inability to account for quantum effects like zero-point energy. Therefore, a more suitable dynamical method that can incorporate these quantum effects is necessary for the investigation of the dynamics.

4. RPMD dynamics

The best candidate for including effects such as zero-point energy in the dynamics is the ring polymer molecular dynamics (RPMD), introduced by Craig and Manolopoulos,^[56–60] which include ZPE^[61] and tunneling^[62] effects. This method has been used successfully to describe reaction dynamics for various profiles of different reaction paths,^[60] using the RPMDrate code.^[46] Recently, a new version based on a direct collision implementation (dRPMD code) has been proposed^[31,45] which has been applied to several reactions with wells and barriers.^[31,36,63] In all these cases, including $\text{H}_2\text{CO} + \text{OH}$ and CH_3OH reaction with OH, RPMD calculations below 200 K are affected by the trapping problem, *i.e.* the formation of a complex between the reactants that live so long that makes it impossible to finish the dynamical study. Thus, to get the total reactive rate constant a combination of RPMD results and RRKM method was used, in which the fraction corresponding to the trapping in RPMD method is distributed among the different reactive or redissociation channels using RRKM theory. It was found that the trapping in RPMD occurs at low temperatures in reactions with wells when the frequencies associated to the beads and the physical low intermolecular frequencies become of the same order.^[36] The trapping was then associated to the spurious resonance problem detected in RPMD simulation of spectra.^[64,65]

4.1. Trapping and thermostated RPMD

One alternative to solve this problem is thermostated RPMD (t-RPMD), in which the beads are “shaken” with an Ornstein-Uhlenbeck thermostat which does not affect the RPMD centroid.^[65,66] This method has been implemented in the dRPMD code, and calculations for different temperatures have been performed for the monomer reaction, $\text{H}_2\text{CO} + \text{OH}$ collisions. These are compared with the results obtained with normal RPMD, as shown in Figure 6 for the direct and trapping probabilities. The results are not completely the same, but they show a similar pattern, so that the differences can also be attributed to statistics. In fact, the equivalence of the two methods was studied by Hele and Suleimanov,^[67] who arrived to a similar conclusion.

To further analyze the differences between RPMD and t-RPMD, in Figure 7 the mean energies obtained in some selected RPMD and t-RPMD trajectories are shown, which depend on the collision times. Clearly when the RPMD or t-RPMD trajectories end normally, the average energy remains similar to the initial one. However, when the mean energy decreases below, typically 0.9 eV for all the temperatures analysed, the trajectory is trapped.

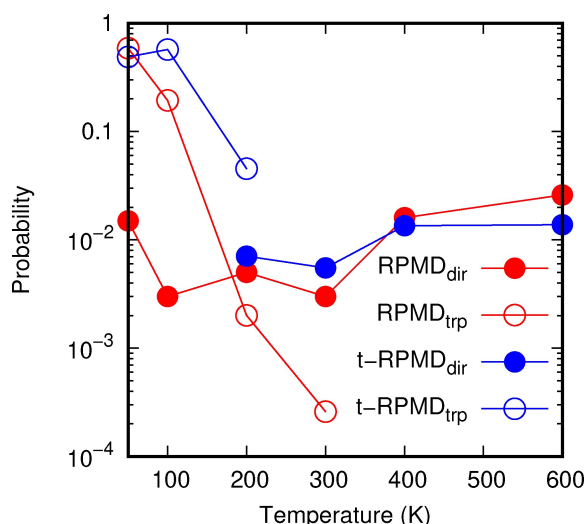


Figure 6. Direct reaction probabilities and trapping probabilities obtained with the RPMD and t-RPMD methods for the $\text{H}_2\text{CO} + \text{OH} \rightarrow \text{HCO} + \text{H}_2\text{O}$ reaction.

At this point, PIMD calculations performed at 50 K for the $\text{H}_2\text{CO}-\text{OH}$ complex yielded an energy of ≈ 0.8 eV, while that of $\text{H}_2\text{CO} + \text{OH}$ constrained to be separated by 50 Å is ≈ 0.96 eV. Clearly, for the trajectories shown in Figure 7 the initial energy corresponds to that of the two reactants separated, including the ZPE. However, when the trajectories become trapped it is because their mean energy approaches that of the $\text{H}_2\text{CO}-\text{OH}$ complex. This is taken as an evidence that RPMD and t-RPMD become equivalent to PIMD calculations. This means that when the frequencies of the beads and those of the intermolecular interactions become of the same order, the pure RPMD with no thermostat is able to sample the configuration space as if it was a PIMD calculation. This essentially happens for slow dynamics, and therefore complex-forming reactions at low temperatures are expected to show this problem.

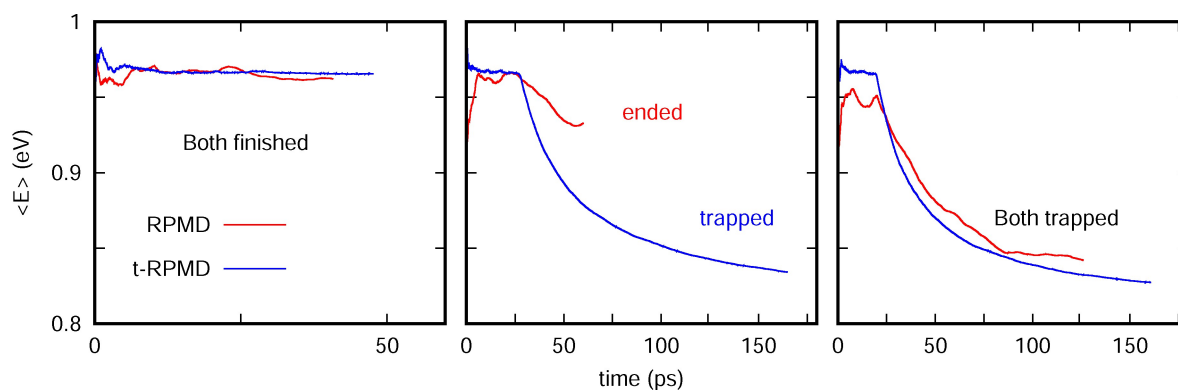


Figure 7. Mean energy obtained for some selected RPMD and t-RPMD trajectories for the $\text{H}_2\text{CO} + \text{OH} \rightarrow \text{HCO} + \text{H}_2\text{O}$ reaction at 50 K.

4.2. RPMD results

The reaction dynamics for the $(\text{H}_2\text{CO})_2 + \text{OH}$ and $\text{H}_2\text{CO} + \text{OH} + \text{H}_2\text{CO}$ have been studied with the RPMD method for 100, 200 and 300 K, using 768, 384 and 128 beads, respectively. 5000 RPMD trajectories are run in each case, with much larger statistical error than QCT calculations, due to the high computational cost of these quantum calculations. The results obtained are shown in Figure 8.

The results for $(\text{H}_2\text{CO})_2 + \text{OH}$ collisions, in the left panels of Figure 8, are in rather good agreement with the QCT results of Figure 5, except for 100 K, for which the RPMD reactive rate (bottom left panel) is about 2 times larger than the QCT results. The reaction rate constant, in the bottom left panel, increases with decreasing temperature from 300 K to 100 K. For lower temperatures, however, the trapping problem makes it infeasible to obtain the RPMD rates and some methodological development is needed to study the lower temperature range to determine if the reaction rate becomes nearly constant. Meanwhile, and based on the qualitative agreement between QCT and RPMD, we can expect that a similar behavior is hold below 100 K. Thus, the reactivity of the $(\text{H}_2\text{CO})_2$ with OH is too low to explain the fast increase of the measured rate constants, as discussed above.

Concerning $(\text{H}_2\text{CO})_2 + \text{OH}$ collisions, the dominant channel is the formation of the $\text{H}_2\text{CO}-\text{OH}$ complex, the dimer exchange mechanism, which at 200 K is about 10 times larger than the reactive process. This can be taken as an indication that the complexes formed, the trimers in this case, do not live enough as to produce a statistical redistribution of energy, at least for temperatures above 100 K. It should be noted that the threshold to produce $\text{H}_2\text{CO}-\text{OH}$ is higher than the reaction barrier height, and statistical methods like RRKM would predict a larger rate constant for the reactive process producing $\text{HCO} + \text{H}_2\text{O} + \text{H}_2\text{CO}$ or any complex among these products.

As an alternative, can the $\text{H}_2\text{CO}-\text{OH} + \text{H}_2\text{CO}$ collisions be responsible for the rise of the rate constant? The answer is no, as indicated in the right panels of Figure 8, at least for temperatures higher than 100 K. As can be seen in the bottom-right panel of Figure 8, the reactive rate in this case is lower at 300 K, and it increases as temperature decreases to 100 K.

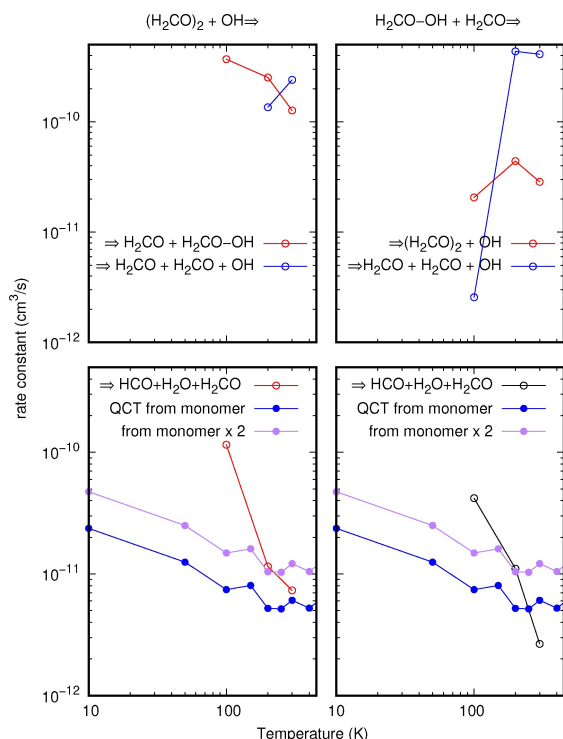


Figure 8. Top panels: rate constant for the formation of: left) $(\text{H}_2\text{CO})_2 + \text{OH} \rightarrow \text{H}_2\text{CO-OH} + \text{H}_2\text{CO}$, and total fragmentation in $\text{H}_2\text{CO} + \text{H}_2\text{CO} + \text{OH}$, and right) $\text{H}_2\text{CO-OH} + \text{H}_2\text{CO} \rightarrow (\text{H}_2\text{CO})_2 + \text{OH}$ and total fragmentation. Bottom panels: Total reactive rate constants obtained for the $(\text{H}_2\text{CO})_2 + \text{OH}$ (left panel) and $\text{H}_2\text{CO-OH} + \text{H}_2\text{CO}$ (right panel) collisions as a function of temperature obtained here with the RPMD method. The QCT results obtained for the monomer in $\text{H}_2\text{CO} + \text{OH}$ collisions are also shown for comparison.^[36]

However, the ratio between the rate constants for the reaction of the two dimers is lower than 2. Taking the risk of making the prediction that the rate constant for the $\text{H}_2\text{CO-OH} + \text{H}_2\text{CO}$ reaction is becoming nearly constant below 100 K, we can then conclude that the reactivity of the dimers, either $(\text{H}_2\text{CO})_2$ or $\text{H}_2\text{CO-OH}$, cannot explain the important rise of the reaction rate constant measured below 100 K. However, it is necessary to conduct additional experimental and theoretical research to confirm this conclusion.

5. Conclusions

In this work we have studied the collision reaction dynamics of dimers to check their role at low temperature in Laval expansion experiments beyond statistical assumptions. For this purpose, a full PES has been developed, depending on all degrees of freedom. This potential is constructed with a matrix force field describing all rearrangement channels and 6 body neural-network terms developed previously to describe the monomer reaction, fitted to reproduced RCCSD(T)-F12a results. The new PES reproduces pretty well *ab initio* calculations at stationary points along reaction paths. In particular, relevant features such as the submerged barrier stabilized by the presence of the second formaldehyde are well described.

The ZPE of the fragments, including monomers and dimers, has been computed using a PIMD method, to establish the energy diagram at low temperatures accurately. These ZPE are also used in QCT dynamical calculations to determine the initial conditions through the adiabatic switching method, and to impose ZPE conditions to the products. The $(\text{H}_2\text{CO})_2 + \text{OH}$ rate constants towards different fragmentation pathways have been first calculated using a QCT method. It is found that the dimer reactive rate constants (producing $\text{HCO} + \text{H}_2\text{O} + \text{H}_2\text{CO}$ and their dimers) are higher than those of the monomer. However, at 10 K the ratio is only twice larger, becoming about 8 times larger at 100 K, and then decreasing again for higher temperatures. These differences are not large enough to explain the important rise on the measured rate constants as temperature decreases.

Since the main product at low temperature is $\text{H}_2\text{CO-OH}$, in the dimer exchange mechanism, the reactivity in the $\text{H}_2\text{CO-OH} + \text{H}_2\text{CO}$ collisions was also analysed. It is found that the QCT method is not able to describe this case, because of the instability of the $\text{H}_2\text{CO-OH}$ complex in QCT calculations, which suffers unphysical energy transfer violating ZPE. Any correction in this classical picture leads to poor statistical results, rendering them unreliable.

RPMD calculations are used as a natural alternative to the QCT method. However, in these complex forming reactions, RPMD is found to yield very high trapping probabilities below 100 K,^[36] i.e. RPMD trajectories that become trapped in the complex and never end. This problem is further analyzed here, finding that when the normal-mode frequencies of the beads become close to those of the reaction complex, they act as an efficient thermostat, thus converting RPMD in a PIMD, not able to describe slow dynamics at low temperatures below 100 K.

For this reason, RPMD calculations are only performed for 100, 200 and 300 K, for the $(\text{H}_2\text{CO})_2 + \text{OH}$ and $\text{H}_2\text{CO-OH} + \text{H}_2\text{CO}$ reactions. In the first case, nearly quantitative agreement with QCT calculations is found. The RPMD rate constants obtained for the $\text{H}_2\text{CO-OH} + \text{H}_2\text{CO}$ reaction are qualitatively very similar to those found for $(\text{H}_2\text{CO})_2$ dimer. Based on the good agreement with the QCT results, we can anticipate that the rate constants will tend to stabilize below 100 K. This is mainly because the effective dipole moment of either of the two dimers diminishes relative to formaldehyde alone. Moreover, the low reaction barrier of the PES would be the dominant reaction mechanism if a complete randomization of energy was produced in the collision complex, as assumed in RRKM method, while in the present dynamical calculations the dominant mechanism at low temperatures is the dimer-exchange with higher energy threshold. Nevertheless, more theoretical work is needed to develop methods for this relatively high number of atoms, that include quantum effects at temperatures below 100 K for complex forming reactions, where RPMD method seems to fail.

Acknowledgements

The research leading to these results has received funding from MICINN (Spain) under grant PID2021-122549NB-C21 and -C22,

and PID2019-107115GB-C21. We acknowledge the computing grants from the "Red Española de Supercomputación" under grants QH-2021-2-0019 (Calendula), AECT-2021-1-0011 (Cibeles) and AECT-2020-1-0003 (Marenostrom). We also acknowledge computing time at Drago (CSIC) and Finisterre III (CESGA).

Conflict of Interests

The authors declare no conflict of interest.

Data Availability Statement

The data that support the findings of this study are available from the corresponding author upon reasonable request.

- [1] R. J. Shannon, M. A. Blitz, A. Goddard, D. E. Heard, *Nat. Chem.* **2013**, *5*, 745.
- [2] J. C. Gómez-Martín, R. L. Caravan, M. A. Blitz, D. E. Heard, J. M. C. Plane, *J. Phys. Chem. A* **2014**, *118*, 2693.
- [3] R. L. Caravan, R. J. Shannon, T. Lewis, M. A. Blitz, D. E. Heard, *J. Phys. Chem. A* **2015**, *119*, 7130.
- [4] M. Antiñolo, M. Agúndez, E. Jiménez, B. Ballesteros, A. Canosa, G. E. Dib, J. Albadalejo, J. Cernicharo, *Astrophys. J.* **2016**, *823*, 25.
- [5] A. J. Ocaña, E. Jiménez, B. Ballesteros, A. Canosa, M. Antiñolo, J. Albadalejo, M. Agúndez, J. Cernicharo, A. Zanchet, P. del Mazo, O. Roncero, A. Aguado, *Astrophys. J.* **2017**, *850*, 28.
- [6] D. E. Heard, *Acc. Chem. Res.* **2018**, *51*, 2620.
- [7] A. J. Ocaña, S. Blázquez, A. Potapov, B. Ballesteros, A. Canosa, M. Antiñolo, L. Vereecken, J. Albadalejo, E. Jiménez, *Phys. Chem. Chem. Phys.* **2019**, *21*, 6942.
- [8] A. J. Remijan, J. M. Hollis, L. E. Snyder, P. R. Jewell, F. J. Lovas, *Astrophys. Lett.* **2006**, *643*, L37.
- [9] A. Bacmann, V. Taquet, A. Faure, C. Kahane, C. Ceccarelli, *Astron. Astrophys.* **2012**, *541*, L12.
- [10] J. Cernicharo, N. Marcelino, E. Roueff, M. Gerin, A. Jiménez-Escobar, G. M. Muñoz Caro, *AstroPhys. J. Lett.* **2012**, *759*, L43.
- [11] C. Vastel, C. Ceccarelli, B. Lefloch, R. Bachiller, *AstroPhys. J. Lett.* **2014**, *795*, L2.
- [12] R. L. Hudson, M. H. Moore, *Icarus* **1999**, *140*, 451.
- [13] N. Watanabe, O. Mouri, A. Nagaoka, T. Chigai, A. Kouchi, V. Pirronello, *Astrophys. J.* **2007**, *668*, 1001.
- [14] R. T. Garrod, E. Herbst, *A&A* **2006**, *457*, 927.
- [15] L. E. Snyder, D. Buhl, B. Zuckerman, P. Palmer, *Phys. Rev. Lett.* **1969**, *22*, 679.
- [16] J. A. Ball, C. A. Gottlieb, A. E. Lilley, H. E. Radford, *Astrophys. J.* **1970**, *162*, L203.
- [17] C. A. Gottlieb, P. Palmer, L. J. Rickard, B. Zuckerman, *Astrophys. J.* **1973**, *182*, 699.
- [18] P. D. Godfrey, R. D. Brown, B. J. Robinson, M. W. Sinclair, *Astrophys. Lett.* **1973**, *13*, 119.
- [19] S. Cazaux, M. Minissale, F. Dulieu, S. Hocuk, *Astron. Astrophys.* **2016**, *585*, A55.
- [20] Y. Oba, T. Tomaru, T. Lamberts, A. Kouchi, N. Watanabe, *Nature Astronomy* **2018**, *2*, 228.
- [21] M. Mainitz, C. Anders, H. M. Urbassek, *A&A* **2016**, *592*, A35.
- [22] G. A. Cruz-Díaz, R. Martín-Doménech, G. M. Muñoz-Caro, Y.-J. Chen, *Astron. Astrophys.* **2016**, *592*, 68.
- [23] M. Bertin, C. Romanzin, M. Doronin, L. Philippe, P. Jeseck, N. Ligterink, H. Linnartz, X. Michaut, J.-H. Fillion, *AstroPhys. J. Lett.* **2016**, *817*, L12.
- [24] A. I. Vasyunin and P. Caselli and F. Dulieu and I. Jiménez-Serra, *Astrophys. J.* **2017**, *842*, 33.
- [25] D. Quénard, I. Jiménez-Serra, S. Viti, J. Holdship, A. Coutens, *MNRAS* **2018**, *474*, 2796.
- [26] S. Zeng, I. Jiménez-Serra, V. Rivilla, S. Martín, J. Martín-Pintado, M. Requena-Torres, J. Armijos-Abendaxiño, D. Riquelmexi, R. Aladro, *NRAS* **2018**, *478*, 2862.
- [27] C. Codella and C. Ceccarelli and P. Caselli and N. Balucani and V. Barone and F. Fontani and B. Lefloch and L. Podio and S. Viti and S. Feng and R. Bachiller and E. Bianchi and F. Dulieu and I. Jiménez-Serra and J. Holdship and R. Neri and J. E. Pineda and A. Pon and I. Sims and S. Spezzano and A. I. Vasyunin and F. Alves and L. Bizzocchi and S. Bottinelli and E. Caux and A. Chacón-Tanarro and R. Choudhury and A. Coutens and C. Favre and P. Hily-Blant and C. Kahane and A. Jaber Al-Edhari and J. Laas and A. López-Sepulcre and J. Ospina and Y. Oya and A. Punanova and C. Pizzarini and D. Quénard and A. Rimola and N. Sakai and D. Skouteris and V. Taquet and L. Testi and P. Theulxié and P. Ugliengo and C. Vastel and F. Vazart and L. Wiesenfeld and S. Yamamoto, *Astron. Astrophys.* **2017**, 605.
- [28] L. G. Gao, J. Zheng, A. Fernández-Ramos, D. G. Truhlar, X. Xu, *J. Am. Chem. Soc.* **2018**, *140*, 2906.
- [29] T. L. Nguyen, B. Ruscic, J. F. Stanton, *J. Chem. Phys.* **2019**, *150*, 084105.
- [30] W. Siebrand, Z. Smedarchina, E. Martínez-Núñez, A. Fernández-Ramos, *Phys. Chem. Chem. Phys.* **2016**, *18*, 22712.
- [31] P. del Mazo-Sevillano, A. Aguado, E. Jiménez, Y. V. 10 Suleimanov, O. Roncero, *J. Phys. Chem. Lett.* **2019**, *10*, 1900.
- [32] F. Naumkin, P. del Mazo-Sevillano, A. Aguado, Y. Suleimanov, O. Roncero, *ACS Earth and Space Chem.* **2019**, *3*, 1158.
- [33] P. Asselin and P. Soulard and B. Madebene and M. Goubet and T. R. Huet and R. Georges and O. Pirali and P. Roy, *Phys. Chem. Chem. Phys.* **2014**, *16*, 4797.
- [34] C. Li and J. Krohn and N. Lippe and R. Signorelli, *Sci. Adv.* **2021**, *7*, eabd9954.
- [35] R. Georges, Personal communication **2021**.
- [36] P. del Mazo-Sevillano, A. Aguado, O. Roncero, *J. Chem. Phys.* **2021**, *154*, 094305.
- [37] A. Zanchet, P. del Mazo, A. Aguado, O. Roncero, E. Jiménez, A. Canosa, M. Agúndez, J. Cernicharo, *Phys. Chem. Chem. Phys.* **2018**, *20*, 5415.
- [38] MOLPRO is a package of ab initio programs designed by H. -J. Werner and P. J. Knowles and with contributions from, J. Almlöf and R. D. Amos and A. Berning and M. J. O. Deegan and F. Eckert and S. T. Elbert and C. Hampel and R. Lindh and W. Meyer and A. Nicklass and K. Peterson and R. Pitzer and A. J. Stone and P. R. Taylor and M. E. Mura and P. Pulay and M. Schütz and H. Stoll and T. Thorsteinsson and D. L. Cooper version **2012**.
- [39] K. Peterson, H.-J. Werner, *J. Chem. Phys.* **2008**, *128*, 084102.
- [40] G. A. Dolgonos, *Chem. Phys. Lett.* **2013**, *585*, 37.
- [41] E. Van Dornshuld, C. M. Holy, G. S. Tschumper, *J. Phys. Chem. A* **2014**, *118*, 3376.
- [42] F. J. Lovas, R. D. Suenram, L. H. Coudert, T. A. Blake, K. J. Grant, S. E. Novick, *J. Chem. Phys.* **1990**, *92*, 891.
- [43] H. R. Barry, L. Corner, G. Hancock, P. R. T. L. Ranson, G. A. D. Ritchie, *Phys. Chem. Chem. Phys.* **2003**, *5*, 3106.
- [44] M. Ceriotti, D. E. Manolopoulos, *Phys. Rev. Lett.* **2012**, *109*, 100604.
- [45] Y. V. Suleimanov, A. Aguado, S. Gómez-Carrasco, O. Roncero, *J. Phys. Chem. Lett.* **2018**, *9*, 2133.
- [46] Y. Suleimanov, J. Allen, W. Green, *Comput. Phys. Commun.* **2013**, *184*, 833.
- [47] J. Andersen, A. Voute, D. Mührin, J. Heimdal, R. W. Berg, M. Tosson, R. Wugt Larsen, *J. Chem. Phys.* **2017**, *146*, 244311.
- [48] C. Sanz-Sanz, A. Aguado, O. Roncero, F. Naumkin, *J. Chem. Phys.* **2015**, *143*, 234303.
- [49] A. Zanchet, O. Roncero, N. Bulut, *Phys. Chem. Chem. Phys.* **2016**, *18*, 11391.
- [50] L. F. Shampine, M. K. Gordon, DDEABM is a driver for a modification of the code ODE written by L. F. Shampine and M. K. Gordon Sandia Laboratories Albuquerque, New Mexico 87185 **1975**.
- [51] M. Karplus, R. N. Porter, R. D. Sharma, *J. Chem. Phys.* **1965**, *43*, 3259.
- [52] T. P. Grodzanov, E. A. Solov'ev, *J. Phys. B* **1982**, *15*, 1195.
- [53] C. Qu, J. M. Bowman, *J. Phys. Chem. A* **2016**, *120*, 4988.
- [54] T. Nagy, G. Lendvay, *J. Phys. Chem. Lett.* **2017**, *8*, 4621.
- [55] M. Braunstein, L. Bonnet, O. Roncero, *PCCP* **2022**, *24*, 5489.
- [56] I. R. Craig, D. E. Manolopoulos, *J. Chem. Phys.* **2004**, *121*, 3368.
- [57] I. R. Craig, D. E. Manolopoulos, *J. Chem. Phys.* **2005**, *122*, 084106.
- [58] I. R. Craig, D. E. Manolopoulos, *J. Chem. Phys.* **2005**, *123*, 034102.
- [59] Y. V. Suleimanov, R. Collepardo-Guevara, D. E. Manolopoulos, *J. Chem. Phys.* **2011**, *134*, 044131.
- [60] Y. V. Suleimanov, F. J. Aoiz, H. Guo, *J. Phys. Chem. A* **2016**, *120*, 8488.
- [61] R. Pérez de Tudela, F. J. Aoiz, Y. V. Suleimanov, D. E. Manolopoulos, *The Journal of Physical Chemistry Letters* **2012**, *3*, 493.

- [62] R. Pérez de Tudela, Y. V. Suleimanov, J. O. Richardson, V. Sáez Rábanos, W. H. Green, F. J. Aoiz, *The Journal of Physical Chemistry Letters* **2014**, *5*, 4219.
- [63] N. Bulut, A. Aguado, C. Sanz-Sanz, O. Roncero, *J. Phys. Chem. A* **2019**, *123*, 8766.
- [64] A. Witt, S. D. Ivanov, M. Shiga, H. Forbert, D. Marx, *J. Chem. Phys.* **2009**, *130*, 194510.
- [65] M. Rossi, M. Ceriotti, D. E. Manolopoulos, *J. Chem. Phys.* **2014**, *140*, 234116.
- [66] M. Ceriotti, M. Parrinello, T. E. Markland, D. E. Manolopoulos, *J. Chem. Phys.* **2010**, *133*, 124104.
- [67] T. J. H. Hele, Y. V. Suleimanov, *J. Chem. Phys.* **2015**, *143*, 074107.

Manuscript received: April 24, 2023
Revised manuscript received: May 25, 2023
Accepted manuscript online: June 16, 2023
Version of record online: June 27, 2023